VLA-GBT Wide-band Galactic Plane Survey

S. Bhatnagar (NRAO), U. Rau (NRAO), M. Rupen (NRAO),
D.A. Green (Cambridge, UK), R. Kothes (DRAO), A. Roshi (NRAO),
S.M. Dougherty (DRAO), P. Palmer (Chicago)

Nov. 30, 2013

Abstract

In this white paper we discuss strategies for a wide-band continuum and spectral line galactic plane survey in the l-band exploiting the power of the vla's widar correlator for simultaneous high resolution observations of the h i 21cm line, all four oh transitions, 18 radio recombination lines (both h and c), and the 1066 mhz transition of formaldehyde. All other existing surveys of the galactic plane in the radio bands are narrow-band surveys. This new survey, using the wide-band capabilities of the evla, besides being able to provide significantly deeper and higher resolution images (up to 10× improvement over cgps in sensitivity and $2-3\times$ improvement in resolution), will for the first time also provide spectral index (si) and rotation measure (rm) maps. The si and rm maps will be the new scientific products (as against improvements over existing products) not available via existing surveys. To allow sensitivity-limited wide-band reconstruction of the omnipresent extended emission and the spatially resolved spectral distribution in the plane, we will also combine these evla observations with similar wide-band observations with the gbt using the vegas back-end.

New development in imaging algorithms enable these capabilities by allowing correction for the frequency and time-variable antenna primary beams and reconstruction of the spectral index distribution even for the extended emission at full spatial resolution (as against at the resolution at the low-frequency end of the observing band). Our experience with processing data from two earlier pilot projects (project id vla/10a-148, VLA/11B-157 and GBT/12A-355 & GBT/14A-252) and careful numerical simulations we have done, suggests that the wide-band mosaic imaging performance for total power and spectral index mapping is excellent, all the required algorithmic components exist and the extra computing load looks tractable. Further work is in progress to adopt and deploy these algorithms on High Performance Computing (HPC) platforms to counter the increased computing resources required by these advanced algorithms. Developing an automated (or semi-automated) imaging pipeline and reliable automatic RFI removal remains a challenge, but looks possible with some extra effort.

We include brief description of some of the scientific goals possible with such a survey. The focus however is more on the design of the survey and the logistics of producing the scientific products. The scientific goals described here are therefore not intended to be exhaustive and written in relatively general terms. Similarly, collaboration with other groups with similar interests and useful expertise in related areas will also be explored depending on the outcome of the VLA Sky Survey evaluation process.

1 Introduction

Large-area surveys of the Milky Way at many wavelengths have shown that the Galaxy is both dynamic and complex, on scales ranging from arcseconds to many degrees. The radio continuum is no exception, being comprised of a rich mix of thermal and non-thermal emission, tracing young stars and supernova remnants, shock waves and magnetic fields. The very richness that makes radio images interesting makes their interpretation challenging since the low radio opacity means that a radio image represents the sum of all emission regions along the line-of-sight – especially in the Galactic Plane. These challenges make the existing narrow-band radio surveys difficult to interpret.

In principle, radio observations can be used directly to disentangle all these effects. Mapping the frequency dependence of the brightness distribution can distinguish free-free from synchrotron emission, mapping polarization at high frequency resolution can constrain the RM along the line-of-sight and mapping the distribution of h i 21cm line and radio recombination lines (RRL) can help map out the three-dimensional distribution of the gas in the Galaxy. All of these however require wide instantaneous bandwidth observations.

To date, only a fraction of this potential has been realized. Existing unbiased radio surveys mostly cover a narrow frequency range with continuum emission a happy afterthought (The Canadian Galactic Plane Survey (CGPS), Taylor et al. (2003)), the ATCA (The Southern Galactic Plane Survey (SGPS), McClure-Griffiths et al. (2005); Haverkorn et al. (2006)) and the VLA (The VLA Galactic Plane Survey (VGPS), Stil et al. (2006)). **While these surveys provide continuum images, the continuum sensitivity of these surveys is severely limited by this narrow total bandwidth. Such narrow bandwidth data also rule out any possibility of deriving a systematic map of the continuum spectral index mapping, RM mapping or building line sensitivities by stacking multiple RRL transitions.**

The EVLA's WIDAR correlator and the new wide-band wide-field imaging algorithms together now open up the possibility of lifting all these restrictions. We can record data for continuum emission over a 2:1 bandwidth ratio, with high spectral resolution and full polarization information, while simultaneously obtaining much higher spectral resolution on interesting parts of the spectrum. The MS-MFS (Rau et al. 2009; Rau 2010), A-Projection (Bhatnagar et al. 2008) and WB-A-Projection (Bhatnagar et al. 2013) algorithms together enable wide-band wide-field imaging that simultaneously give high quality continuum and spectral index maps of regions with complex emission (see Figs. 1 and 2).

In this white paper, we discuss observing and data processing strategies for a wide-band survey of the Galactic Plane at L-Band in D-array with simultaneous recording of continuum data along with higher frequency-resolution data centered on the H I 21cm line, OH lines and 18 RRL transitions within the L-Band. We also discuss the advantages and disadvantages of including S-Band and C-array to improve resolution and frequency coverage as well as distributing the observing over time to get cadence of years, weeks and days to make transient-science possible with this data set. To reliably reconstruct the large scale emission in total intensity and spectral distribution, we will also combine similar wide-band observations with the GBT. As a proof-of-concept demonstration, we include results from our two pilot projects for deep wide-band single pointing and mosaic imaging in the Galactic Plane.

2 Scientific Goals

2.1 Continuum and Spectral Index imaging

Supernova explosions have a profound effect on the morphology, kinematics, and ionization balance of galaxies, and possibly trigger new generations of star formation. However, based on statistical studies of predicted SNR rates, there should be many more SNRs in our Galaxy (1,000–2,000; Li et al. 1991, Tammann, Loeffler, & Schroeder 1994) than are currently known (~ 274; Green (2009)). *In addition to this deficit in the total count, current catalogues also lack young (and hence small) remnants.* The missing remnants are thought to be concentrated toward the inner Galaxy where the diffuse synchrotron emission from the Galactic ridge and H II regions cause the most confusion.

Observations of low-frequency (< 2 GHz) Radio Recombination Lines (RRLs) established the presence of extended low-density ionized gas (DIG) in the inner Galaxy ($|l| < 50°$) (Lockman 1976; Anantharamaiah 1985; Pedlar et al. 1989), Roshi & Anantharamaiah (2000) showed that the line emission is clumpy (at scales of a few arcmin) but extended (few degree scale). Studies of radio free-free emission suggest that the DIG is ionized via absorption of > 70% of the radiation from OB stars, while 'classical' H II regions absorbing the rest (Mezger 1978; McKee & Williams 1997; Murray & Rahman 2010). *Thus, while the DIG plays an important role in the evolution of the ISM, we still do not know how the photons from OB stars travel long distances beyond the 'classical' H II regions to ionize the DIG.* A detailed observational study of the morphology of the DIG can give clues to answer this question and test the various morphological models proposed in the literature (Shaver 1976; Anantharamaiah 1986; Heiles et al. 1996; Murray & Rahman 2010). *The expected thermal emission from DIG is in the range* $0.8 - 4.8K$.

Unbiased wide-band continuum and spectral index mapping can separate thermal and non-thermal emission and help identify the missing populations of SNRs as well as differentiate the thermal nature of the DIG from diffuse non-thermal emission at high significance.

2.2 RM-synthesis

Spatially resolved Rotation Measure (RM) maps provide not only the spatial distribution of Faraday rotation screens, but also a handle on the Faraday depth distribution by separating the emission at different depths. Smooth background polarization is produced everywhere in our Galaxy and it is Faraday rotated while it is propagating through the Galaxy. With RM synthesis we can determine the Faraday rotation seen by different sources of polarized emission along the line of sight. **With the large number of compact background sources seen through the Galaxy, we can also separate their internal Faraday rotation from the foreground rotation, produced by our Galaxy, using RM synthesis**.

2.3 Spectral Line Science

RRL: In the 1–2 GHz frequency range, the hydrogen alpha RRLs from classical H II regions (i.e T~7000K) are expected to be 1-2% of the continuum. At the sensitivity level we expect to attain, lines will exceed 5 sigma for several known sources in the field-of-view. *Because we will observe 18 lines over the frequency range, we will also be able to separate optical depth effects and non-LTE effects.* **Note that for weaker line search, we will be able to stack sub-bands to improve sensitivity at the cost of losing information about variation of non-LTE effects.**

OH: The 4 L-band lines of OH are very useful probes of the interstellar medium. The 1665 and 1667 MHz ("main lines") are often masers in regions of high density and excitation in regions of star formation. The 1720 MHz masers are frequently found on the rims of supernova remnants, while the 1612 MHz masers are often found in the circumstellar shells around Red Supergiants. Absorption in all 4 lines occurs in less dense gas along the line of sight to radio sources, and all four lines are also detected in cold dust clouds. **The versatility of the WIDAR correlator permits simultaneous observation of these lines to sample a wide range of interstellar conditions.**

H_2CO: We propose to include the $4_{22} - 4_{23}$ transition of H_2CO at 1.066 GHz in one narrow subband. This line will not be found in the general ISM because both the upper and lower states can also decay by spontaneous transitions with lifetimes $\sim$ 2000 sec. Therefore, they will only be populated in regions with densities of $\sim 10^6 \mathrm{cm}^{-3}$ and temperatures $\sim$ 100K, i.e similar to regions of mainline OH masers and H_2O masers. **The excitation of closely spaced K-doublets is delicate, and we have no prediction for the relative populations of the 4_{22} and 4_{23} levels.**

H I : While data from the CGPS, SGPS and VGPS H I surveys exist, our observations will provide higher brightness sensitivity data on the H I line.

We also want to observe lines, in particular the H I line, in linear polarization as well. **Data from existing surveys does not have spectral line data in full polarization, typically due to limitations of the correlator resources.** Since H I emission is unpolarized we have the unique opportunity to observe very clean absorption profiles from sources that are too faint to produce reliable absorption signals in total power. H I absorption in total power is limited by foreground fluctuations of a few Kelvin ($\sim$ 6 K) produced by clouds smaller than the beam. Therefore, only H I absorption profiles of sources with at least 20 K peak brightness can produce significant absorption in total power, no matter how long you integrate. To get a reliable absorption profile we probably need 50 – 100 K peak brightness and even those profiles are sometimes ambiguous. This is in particular true for extended sources. In polarization those profiles are noise limited and there is no ambiguity caused by small-scale fluctuations. A preliminary study of this was done by (Kothes et al. 2004). They did detect H I absorption in polarization of SNRs that have $\sim$ 1 K peak brightness in polarization. This method would be great to determine distances to Galactic SNRs and probe the ISM with polarized extragalactic sources.

3 Observing Strategy

3.1 Observing Frequency

Radio emission from the Galactic Plane has a rich mix of thermal and non-thermal emission. Non-thermal radio emission from the Galactic Plane (e.g. from SNRs) is synchrotron radiation which has a power-law dependence on frequency with a negative spectral index α ($S \propto \nu^{\alpha}$). This makes the emission stronger at lower frequencies, peaking at frequencies of few$\times$100 MHz and progressively weakens with increasing frequency. Thermal emission (e.g. from typical H II regions) on the other hand has a flat spectrum above $\sim$1 GHz. Below this frequency the optical depth is much greater than 1 and the spectrum turns over with a spectral index of $\sim$ 2.

Low-frequency RRL emission ($<$ 2 GHz) provides a unique probe of the DIG component of the ISM. In the 1 – 2 GHz range, 18 RRL transitions may allow separation of optical depth effects and non-LTE effects as well as detection of the weaker lines by stacking multiple transitions to gain sensitivity. This frequency range also gives access the H I 21cm line and the four OH transitions and the yet undetected $4_{22} - 4_{23}$ transition of H_2CO at 1.066 GHz.

We therefore suggest that the primary frequency range of the survey be the L-Band covering the 1 – 2 GHz range. Additionally the survey can also be done at S-Band covering a total frequency range of 1 – 4 GHz. Such a L- and S-Band survey will be better optimized for mapping both thermal and non-thermal emission, various line transitions and better spectral index and RM mapping. However, as discussed below, this increases the required time.

3.2 Pointing separation and total observing time

Assuming similar area of the Galactic Plane as covered in the CGPS, the total area of the sky to be imaged is 660 Sq. deg. The CGPS survey used a pointing separation of $1.04 \times FWHM$ (and not $FWHM/2$, as is often advocated to be *required* for mosaic imaging) with minor degradation in the RMS noise. With 2:1 bandwidth ratio, the primary beam (PB) varies in size by a factor of two across the L-Band. The instantaneous wide bandwidth of the EVLA must allow good imaging performance with larger pointing separation. Since the reduction in time can be large, in order to measure the effect of various pointing separation on the imaging performance, we used 15 arcmin ($FWHM/2$ at L-Band) separation between the pointings in our second EVLA RSRO project[1] and GBT project [2] to image a 3×3 Sq. deg. region. This separation is closer than conventionally done for narrow-band

[1] EVLA Project 11B-157; "Simultaneous wide-band and spectral-line mosaic imaging in the Galactic plane", S. Bhatnagar, M. Rupen, U. Rau, D. A. Green, R. Kothes, P. Palmer, A. Roshi, K. Golap, S.M. Dougherty

[2] GBT/12A-355: "Simultaneous wide-band and spectral-line imaging of the Galactic plane", A. Roshi, S. Bhatnagar, M. Rupen, R. Kothes, U. Rao Venkata, D.A. Green, P. Palmer, S. Dougherty & K. Golap

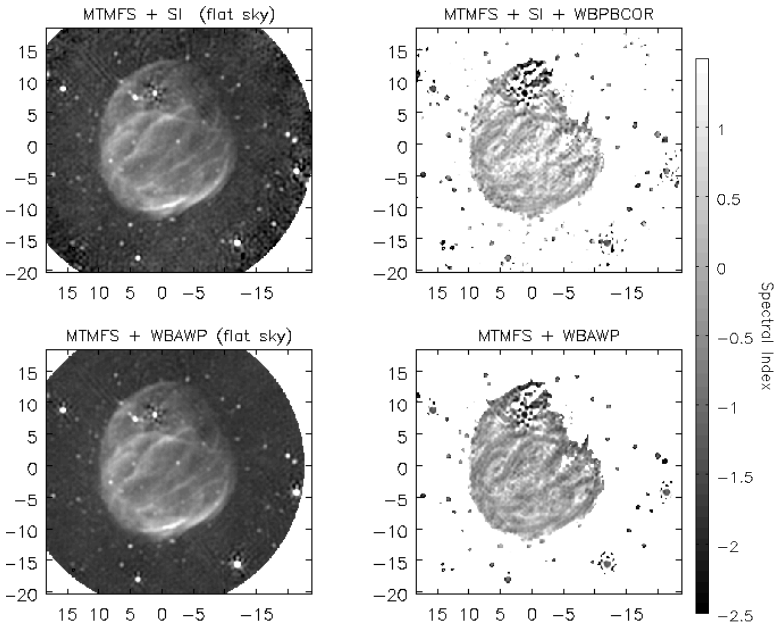

Figure 1: Wide-band continuum and spectral index map of a single pointing observation. The SNR fills the primary beam (PB) at the reference frequency of 1.5 GHz. The top panel shows imaging without PB correction. The steeper spectral index away from the center of the image is due to the frequency dependence of the PB. Poorer reconstruction is due to the time dependence of the PB. Bottom panel shows imaging with PB correction. As a test, the spectral index of the compact source (a pulsar) inside the top edge of the SNR was reconstructed accurately in the spectral index map in the bottom-right panel after PB correction (see Bhatnagar et al. (2013)).

mosaic observations and allowed us to measure imaging performance as a function of pointing separation. Our experiments with imaging algorithms suggest that we can increase the pointing separation to at least 22 arcmin without significant degradation in the total intensity or spectral index mapping performance (see Table 1 below). This is not surprising given that the CGPS used a pointing separation of $1.04 \times FWHM$ and the H I VGPS used a separation of 25 arcmin ($1.3 \times FWHM$). In fact this suggests that at least for continuum imaging, wider separation with corresponding *significant* reduction in observing time may be possible.

This will require 7260 pointings. Via our pilot projects we determine that 10 min. per pointing is sufficient for mapping large scale emission and its spectral index distribution as well as achieve order of magnitude improvement in noise RMS compared to the CGPS. With 7260 pointings the total observing time required is 1331 hr (1210 hr for on-source integration plus 10% overhead). With these parameters, the expected 1-sigma sensitivities are :

- **Continuum imaging:** (8×128MHz) : 35 μJy/b. (Accounting for 20% data loss due to RFI, we get 43 μJy).
- **Line imaging:** (2kHz channel) : 9 and 17 mJy at 1 and 2 GHz respectively (due to the difference in field-of-view overlap across the band).
- **Faraday Depth:** With a total bandwidth of 1 GHz at 1 MHz channel resolution, we will be sensitive to Faraday depths in the range $10 - 25000\ rad/m^2$.

Following is a table showing the expected continuum RMS, its variation across the field with different pointing separation, the associated observing time and number of pointings required.

Frequency Band	Spacing (arcmin)	Number of pointing	Total time (hours)	RMS $\pm\Delta RMS$ ($\mu Jy/b$)
L-Band	15	15675	2874	23 ± 0.3
	22	7260	1331	35 ± 4.3
S-Band	10	31185	5717	22 ± 1.7
	15	15675	2874	35 ± 12

Table 1: Table of observing parameters with associated time, estimated RMS noise and variation in the sensitivity due to pointing separation at L-Band covering the frequency range of $1 - 2$ GHz and at S-Band covering a frequency range of $2 - 4$ GHz.

3.3 Cadences in time for spectral line mapping and transient source detection

While our first pilot project[3] shows that 10 min per pointing integration gives excellent continuum uv-coverage due to instantaneous wide bandwidth, the uv-coverage will be improved for spectral line mapping by making several shorter visits separated in time.

Furthermore, the total integration time per pointing can be built over multiple visits spread over longer time to get time cadences of days, weeks and years for transient emission detection in the Plane. We discuss a few possibilities below.

1. **Build the sensitivity in 5 pieces** in each D-array configuration every ∼1.5 years. The survey therefore completes over 7.5 years. To take an example, with 22 arcmin pointing separation, each piece (each D-array config) needs ∼266 hr of total observing time. This gives the longest cadence of 1.5 years for transient science. In each piece we do 2 min. per pointing and get ∼ 78 ± 9.6μJy/b sensitivity per piece (i.e. per 1.5 years).

   Each piece of 2 min per pointing can be built, say, in 2 or 4 visits (1 min or 0.5 min per pointing). This would give a shorter time cadence of few days for transients per piece at the sensitivity limits of 110 ± 13 and 156 ± 19 $\mu Jy/b$ respectively.

2. **Build the sensitivity in 2 pieces.** This gives two visits separated by 1.5 years, but will allow shorter time cadences of few days *and* weeks.

No. of pieces	Total length (years)	Total time per piece (hr)	RMS per piece ($\mu Jy/b$)	RMS per visit ($\mu Jy/b$)
5	7.5	266	78	110 (2 visits) 156 (4 visits)
2	3.0	665	49	70 (2 visits) 98 (4 visits)

Table 2: Table of achievable RMS per piece with 5 & 2 pieces with 2 or 4 visits per piece.

3.4 Array Configuration

3.4.1 Combining D- and C-array observations at L-band

The maximum baseline length in D-array is comparable to the maximum baseline used for the CGPS which gives a resolution of $\sim 1' \times 1'$. In addition to D-array, which along with single dish data from the GBT allows reliable reconstruction of the large scale emission, adding C-array observations will give a 3× improvement in spatial resolution compared to CGPS at the cost 2× extra observing time. However for the same surface brightness sensitivity the total observing time will increase by 9×. The scientific returns will be in terms of higher spatial resolution and shorter cadences for detection of transient emission (1.5 years for configuration-change cycle, 3-4 months for the change from D- to C-array, and shorter cadence as discussed in Section 3.3 above).

A nine-fold increase in time to cover the same region of sky as covered at L-Band may be prohibitive. An alternate approach could be to survey a smaller part of the Plane in C-array (e.g. the inner quadrant only).

3.4.2 Combining L- and S-band in D-array

A wide frequency coverage can be achieved by conducting the survey in D-array at S-band (*in addition* to L-band). This, together with L-band observations provides frequency coverage of $1-4$ GHz. The advantages would be **(a)** improved resolution by a factor of two (0.5 arcmin), **(b)** improvement in the RMS limit by a factor of $\sqrt{2}$, **(c)** significantly better spectral index reconstruction (due to larger frequency coverage), **(d)** higher sensitivity for RM mapping and **(e)** better optimized survey for mapping both thermal and non-thermal emission. See Table 1 for S-band parameters.

As an example, a survey RMS limit of 35μ**Jy/b corresponding to 22 arcmin separation at L-band can be achieved with a S-band survey with 15 arcmin pointing separation requiring an** *extra* **observing time of 2874 hr. See Fig. 3 for examples of sensitivity patterns and RMS noise across the field at L-Band for pointing separation of 15 and 22 arcmin.**

To achieve same surface brightness sensitivity at higher resolution than D-array@L-Band and also covering the same region of the sky will require 9× **extra observing in the C-array@L-Band. In comparison** 4× **extra observing will be**

[3]EVLA Project 10A-148; "Wideband imaging of Galactic SNRs: A pilot project for a wideband Galactic Plane Survey"; S. Bhatnagar, D.A. Green, U. Rau, M. Rupen, K. Golap, R.A. Perley

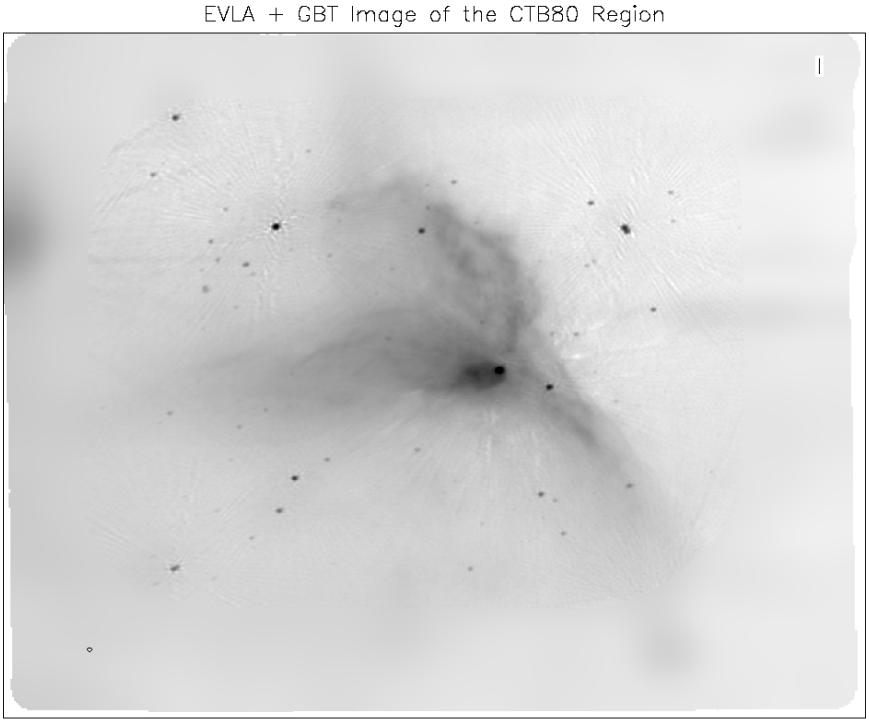

Figure 2: An example of wide-band mosaic imaging of a 3×3 sq. deg. region of the Galactic Plane. This preliminary image from the observations of our RSRO pilot project (VLA/11B-157 and test observations for GBT/12A-355) combines D-array EVLA wide-band data with L-band data from the GBT. Due to an error during imaging, not the entire EVLA was combined with the lower-resolution GBT image resulting in higher level of artifacts in this preliminary image. Further work, including to map the spectral index distribution, possible with the EVLA and GBT data, is currently in progress.

required in D-array@S-Band combination giving a $2\times$ better resolution than D-array@L-Band only. The latter offers an extra advantage of wider frequency coverage which will be a significant and important advantage in the accuracy of spectral index and RM maps. Adding S-band would give us more sensitivity to high rotation measures, which is very important towards the inner Galaxy, in particular close to the Galactic center. It would also give us a better ability to disentangle lines of sight, which show complex Faraday depth structures.

Survey Name	Config & Band	Resolution (arcmin)	RMS ($\mu Jy/b$)	Total time (hr)
CGPS		1×1	300	–
VLA-GBT	D+C@L-Band	0.3×0.3	$35/\sqrt{2}$	1331×2
Fixed surface brightness in D & C array				$1331 + 1331 \times 9$
VLA-GBT	D@L+S-Band	0.5×0.5	$35/\sqrt{2}$	1331 + 2874
Fixed surface brightness at L- and S-Band				$1331 + 2874 \times 4$

Table 3: Table showing the achievable resolution and sensitivity as a function of the required observing time for combinations of D- and C-array at L- and S-Band.

3.4.3 GBT Wide-band data

As shown by the CGPS results as well as in the preliminary result in Fig. 1, combining single dish data with interferometric data, improves the imaging performance significantly. Accurate reconstruction of the spectral index distribution will similarly benefit from combining with wide-band single dish data. Such single dish wide-band data covering the entire L-Band can be obtained with a comparable survey of the Plane with the GBT using the VEGAS band-end. For a GBT survey covering the VLA S-band, we may need only a few narrow-frequencies for the GBT data in the S-band, to derive a good-enough wideband model, especially since the frequency coverage of such a combined survey will go from 1-4 GHz.

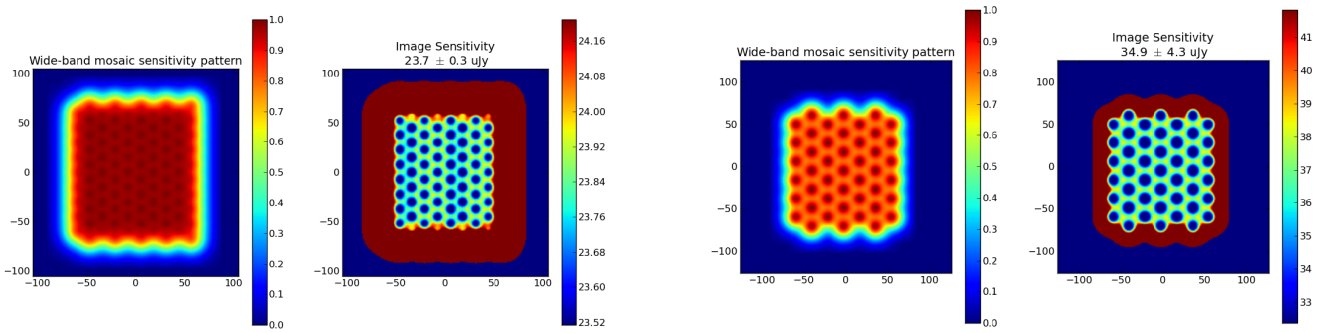

Figure 3: **Left panel**: The first figure shows the sensitivity pattern at L-Band covering an area of 2×2 Sq. deg. with a pointing separation of 15 arcmin, equal to half of the full width at half maxima (FWHM) at the reference frequency of 1.5 GHz. The second figure shows the RMS noise across the field of view.
Right panel: Same figures as in the left panel, but for a pointing separation of 22 arcmin ($1.5 \times FWHM$).

3.5 Correlator setup

For these observations, we will configure the WIDAR correlator to cover the 1–2 GHz frequency range and the rest of the correlator resource to cover the spectral lines. Refer to Table 4 for detailed correlator setup we used in our RSRO Project 11B-157. A simillar setup can be used for the survey discussed here.

Subband	Bandwidth	N^b_{pp}	N_{chan}/sb^c	dv^d	dt^e
RC: 1-8[e]	8×128 MHz	4	128	1 MHz	1 sec
H I -1420 MHz	4 MHz	4	8192	0.49 kHz	32 sec
OH-1612 MHz	4 MHz	2	4096	1 kHz	32 sec
OH-1665/7 MHz	4 MHz	2	16394	0.24 kHz	32 sec
OH-1720 MHz	4 MHz	2	4096	1 kHz	32 sec
H_2CO-1066 MHz	4 MHz	2	4096	1 kHz	32 sec
RRL: 1-18[f]	18×4 MHz	2	8192	0.49 kHz	32 sec

Table 4: [a]N_{pp} is the number of polarization products, [b]Number of channels per subband, [c]Channel separation, [d]Integration time out of the Correlator Backend, [e]Radio continuum subbands, covering the full 1–2 GHz band. The dump time and channel separation are chosen to allow full-beam imaging and RFI excision., [f]Radio recombination lines. There are 39 Hα lines within the 1–2 GHz band; we will choose 18 which are in RFI-free zones and avoid the 128 MHz boundaries set by stage 1 of the subband filters. The 4 MHz subbands are sufficient to include the corresponding He and C lines as well. The C lines can be quite narrow (few km/sec), setting the required channel width. . Details of the correlator configuration. We use both recirculation and Baseline Board stacking. This setup uses 63 of the 64 Baseline Board pairs and gives at total data output rate of $\sim$ 40 MB/sec.

4 Data Processing Strategy

Existing calibration and RFI removal pipelines (or a tuned version of it) will be used for automatic calibration. To fully utilize the bandwidth, may require improvements in the RFI removal. Any improvements in the RFI removal or performance of the calibration pipeline as part of this survey or efforts from other projects can be adopted by all and made available in general.

Imaging with wide-band data in the Galactic Plane requires imaging algorithms which can handle extended as well compact emission, model it as a function of frequency and polarization and account for the time, frequency and polarization dependence of the antenna primary beam. Most of the algorithmic pieces required for this now exist (see details below). Using these algorithms, an imaging pipeline will be developed and deployed on High Performance Computing (HPC) platform for wide-band mosaic imaging required for such a survey.

4.1 Imaging

Combination of wide-band interferometric data with single dish data allows accurate reconstruction of the emission at all scales up to a resolution given by the longest interferometric baseline. Imaging in the Galactic Plane, where reasonably strong extended emission is present in every pointing, requires scale-sensitive algorithms which inherently models the extended emission using better basis functions. With instantaneous wide bandwidths, the emission significantly varies across the band and the antenna primary beam also scales with frequency changing by a factor of two across the band. All these effects, if not corrected for,

produces artifacts many times stronger than the thermal limit in the total intensity, spectral index and RM maps. Imaging algorithm to simultaneously model the emission as a function of frequency and polarization and correction of the primary beam effects which vary with time, frequency and polarization is therefore essential.

The Multi-term Multi-frequency Synthesis algorithm (MT-MFS, Rau & Cornwell (2011)) enables simultaneous mapping of total intensity and spectral index distribution of extended emission in a multi-scale basis. The Wide-Band AW-Projection algorithm (Bhatnagar et al. (2013)) corrects for the time, frequency and polarization dependence of the antenna primary beam. These algorithms together enable the accurate continuum and spectral index mapping with wide-band data in the Galactic Plane even in the presence of large scale emission (see Fig. 1). Work is currently in progress on advanced scientific test of extension of this approach to wide-band mosaic continuum and spectral index mapping. Some initial results from this work are shown in Fig. 2 which shows a wide-band mosaic of the CTB80 region combined with the single dish data from the GBT. This is an initial result and work is in progress to further improve the image as well as map the spectral index distribution. In parallel, work will soon start on implementing similar RM mapping algorithms which have the potential of making RM maps with optimal utilization of the available bandwidth.

All these algorithms will be available in the CASA libraries. We therefore think that the basic algorithms required for such a survey exist and are implemented (or will be implemented) in standard observatory supported software package. The final piece of development required for this survey is to deploy these algorithms on HPC platforms. More work in this area is required and is in progress.

Once the basic algorithms are tested and in place, an imaging pipeline tuned for this survey will be developed and used for automatic imaging.

4.2 Challenges

4.2.1 Computing costs

The MT-MFS algorithm accounts for the frequency dependence of the sky brightness and the WB AW-Projection algorithm corrects for the time, frequency and polarization dependence of the antenna primary beams. Since noise-limited continuum, spectral index and RM mapping requires accounting for all these effects *simultaneously*, the combined MT-MFS+WB AW-Projection algorithm is required to achieve the scientific goals of such a survey. However these algorithms are inherently more compute intensive and can be expected to require at least an order of magnitude more computing. The memory footprint can also be an issue. While hybrid approaches are possible (using narrow-band algorithms to address the wide-band issues), those have been found to be neither sufficient in terms of imaging performance nor less expensive than wide-band algorithms (Rau & Bhatnagar, in prep.).

Computing related to the WB AW-Projection is an embarrassingly parallel problem and can be mitigated to a large extend by deploying the algorithm on cluster computing platforms. Investigations done so far suggest that use of GPU computing can further mitigate the computing costs efficiently. Work is in progress to evaluate these options and preliminary results suggest that a significant part of the MT-MFS algorithm will also benefit in terms of reduced memory footprint and computing cost using GP-GPU. More work is required to take full advantage of GPU computing for the combined algorithm. The results so far are encouraging. If adapting the algorithms for GPUs work out as expected, the benefits in run-time and associated costs will be significantly reduced.

4.2.2 Wide-band Polarization

Accurate RM mapping requires wide-band polarization calibration and accounting for any frequency and direction-dependent instrumental effects. While algorithms and procedures for full-polarization calibration and imaging also exist, these need to be tested carefully. Imaging algorithms better optimized to use the available bandwidth for RM mapping of extended emission as well require some R&D as well. A PhD level student project focused on this problem is in progress and we expect will provide the necessary tools with careful scientific tests of expected performance. Finally, due to large data volumes and higher computing involved, these also have to deployed on HPC platforms.

4.2.3 Transient Detection Algorithms

Here we rely on the work done by various groups on transient detection algorithms and related data processing.

References

Anantharamaiah, K. R. 1985, Journal of Astrophysics and Astronomy, 6, 177
Anantharamaiah, K. R. 1986, Journal of Astrophysics and Astronomy, 131

Bhatnagar, S., Cornwell, T. J., Golap, K., & Uson, J. M. 2008, Astron. & Astrophys., 487, 419
Bhatnagar, S., Rau, U., & Golap, K. 2013, ApJ, 770, 91
Green, D. A. 2009, Bulletin of the Astronomical Society of India, 37, 45
Haverkorn, M., Gaensler, B. M., McClure-Griffiths, N. M., Dickey, J. M., & Green, A. J. 2006, AJ Supp., 167, 230
Heiles, C., Reach, W. T., & Koo, B. 1996, ApJ, 466, 191
Kothes, R., Landecker, T. L., & Wolleben, M. 2004, ApJ, 607, 855
Lockman, F. J. 1976, ApJ, 209, 429
McClure-Griffiths, N. M., Dickey, J. M., Gaensler, B. M., et al. 2005, AJ Supp., 158, 178
McKee, C. F. & Williams, J. P. 1997, ApJ, 476, 144
Mezger, P. O. 1978, Astron. & Astrophys., 70, 565
Murray, N. & Rahman, M. 2010, ApJ, 709, 424
Pedlar, A., Anantharamaiah, K. R., Ekers, R. D., et al. 1989, ApJ, 342, 769
Rau, U. 2010, PhD thesis, The New Mexico Institute of Mining and Technology, Socorro, New Mexico, USA
Rau, U., Bhatnagar, S., Voronkov, M. A., & Cornwell, T. J. 2009, Proc. IEEE (Sp. Issue on Advances in Radio Telescopes), 97
Rau, U. & Cornwell, T. J. 2011, Astron. & Astrophys., 532, A71
Roshi, D. A. & Anantharamaiah, K. R. 2000, ApJ, 535, 231
Shaver, P. A. 1976, Astron. & Astrophys., 47, 49
Stil, J. M., Taylor, A. R., Dickey, J. M., et al. 2006, Astron. J., 132, 1158
Taylor, A. R., Gibson, S. J., Peracaula, M., et al. 2003, Astron. J., 125, 3145